Trilayer Crystalline Lamellar Morphology under Confinement

Tsai-Ming Chung and Rong-Ming Ho*

Department of Chemical Engineering, National Tsing Hua University, Hsinchu 30013, Taiwan

Jing-Chung Kuo and Jing-Cherng Tsai

Department of Chemical Engineering, National Chung Cheng University, Chia-Yi 62142, Taiwan

Benjamin S. Hsiao and Igors Sics

Department of Chemistry, Stony Brook University, Stony Brook, New York 11794-3400

Received December 9, 2005
Revised Manuscript Received March 1, 2006

Crystallization behavior under nanoscale spatial confinement has drawn extensive studies in recent years due to the prerequisite for the basic understanding of crystallization in the applications of nanotechnologies.[1,2] Owing to their representative characters for crystallization under confinement, the crystallization behavior of semicrystalline block copolymers has thus been thoroughly examined.[3−17] The final crystalline morphology was found to be strongly dependent upon the experimental temperature, with respect to the order−disorder transition temperature (T_{ODT}), the crystallization temperature of the crystallizing block (T_c^c), the glass transition of amorphous block (T_g^a), and the crystallization rate.[3] In other words, the final morphology results from the competition between crystallization and microphase separation and can be justified in accordance with the ratio of segregation strength of microphase separation at T_c and at T_{ODT}.[4] In addition, the ordered nanostructure can be preserved due to the vitrified microdomains of amorphous blocks for systems with $T_{ODT} > T_g^a > T_c^c$ (this is a hard confinement for crystallization).[5−9] By contrast, if $T_{ODT} > T_c^c \geq T_g^a$, the effect of crystallization on the morphological changes becomes more complicated (this is a soft confinement).[10−16] The crystalline morphology under confinement and the corresponding molecular dispositions of crystalline chains have thus drawn intensive attention in order to understand the confined crystallization behavior.[6,7,10,11,17] In this Communication, a peculiar crystalline texture under confinement, a trilayer syndiotactic polypropylene (sPP) crystalline lamellar morphology in between vitrified polystyrene (PS) confinement in the polystyrene-*b*-syndiotactic polypropylene (PS−sPP) diblock copolymers, was observed for the first time. We believe that this may provide new insights into crystalline geometrics under nanoscale spatial confinement.

Crystallizable PS−sPP diblock copolymers were synthesized as briefly described below.[18] The number-average molecular weights of PS and sPP were determined as 7400 and 8900 g/mol, respectively, by gel permeation chromatography (GPC) analysis, and the polydispersity (PDI) of PS−sPP was 1.29 as measured. The volume fraction of sPP, calculated by assuming that the densities of PS and sPP are 1.02 and 0.854 g/cm^3, was 0.59 in the molten state. The order−disorder transition temperature, T_{ODT}, was determined as 265 °C by time-resolved SAXS heating experiments.[16] On the basis of the T_{ODT} measurement, the self-assembled microstructure of PS−sPP at the examining temperature range in this study can be considered as a system with strong segregation strength.

Bulk samples of block copolymers were annealed at 180 °C (that is above the sPP melting but below the order−disorder transition temperature) for 5 min and then rapidly cooled at a rate of 150 °C/min to a preset temperature ($T_{c,sPP}$) for isothermal crystallization. Microphase-separated lamellar morphology was found for the quenched sample from the melt as evidenced by transmission electron microscopy (TEM) and small-angle X-ray scattering (SAXS) experiments (not shown). To study the crystallographic details of sPP crystallites grown in between the vitrified PS microdomains (that is, hard confined environment), the microphase-separated melts were subjected to a large-amplitude oscillating shear at 180 °C to achieve a uniform, parallel alignment of the lamellar phase morphology. The shear apparatus was aerated with nitrogen gas to prevent thermal degradation (see Figure 3 for the shear geometry). The shear direction was along the *x* direction, and the shear gradient was along the *z* direction. Following the successful approach by Khan and co-workers, the shear frequency was 0.5 Hz and the shear amplitude was 150%.[8,19]

TEM and electron diffraction (ED) experiments were conducted on a JEOL TEM-1200x instrument. Thin slices of shear-aligned PS−sPP samples having a thickness of about 60 nm were obtained by a Reichert Ultracut microtome at room temperature. Staining was accomplished by exposing the samples to the vapor of a 4% aqueous RuO_4 solution for 30 min. Because of the possibility that RuO_4 may disrupt the crystallinity of the sPP block, electron diffraction experiments were conducted on unstained specimens. Simultaneous 2D SAXS and wide-angle X-ray diffraction (WAXD) experiments were conducted at the synchrotron X-ray beamline X27C at the National Synchrotron Light Source (NSLS) in Brookhaven National Laboratory (BNL). The wavelength of the X-ray beam was 0.1366 nm. A MAR CCD X-ray detector (MAR) was used to collect the 2D SAXS patterns. A 1D linear profile was obtained by integration of the 2D pattern. The scattering angle of the SAXS pattern was calibrated using silver behenate, with the first-order scattering vector q^* ($q^* = 4\pi\lambda^{-1} \sin\theta$, where 2θ is the scattering angle) being 1.076 nm^{-1}. The diffraction peak positions and the widths observed from WAXD experiments were carefully calibrated with silicon powder with 2θ being 28.4° under Cu Kα radiation. Azimuthally integrated profiles were extracted from 2D WAXD patterns for further analysis. Isothermal crystallization measurements were carried out on a customized two-chamber hot stage. The isothermal crystallization temperature (T_c) was controlled to within ±0.1 °C. The samples were preheated to 180 °C in the melting chamber for 5 min and then quenched (switched) to the second chamber with preset temperatures for isothermal crystallization.

Interestingly, the isothermally crystallized sPP crystallites under hard confinement (namely, the crystallization of sPP was carried out within the strong-segregated and vitrified PS microdomains) exhibited an unusual morphology, a trilayer crystalline lamellae in the microphase-separated sPP lamellar microdomains, as illustrated in Figure 1. The PS microdomains appeared relatively dark after preferential staining by RuO_4; by comparison, the amorphous parts of sPP appeared gray after staining, whereas the crystalline parts of sPP exhibited significant contrast as bright regions due to a slow staining rate for

* To whom all correspondence should be addressed: Tel 886-3-5738349; Fax 886-3-5715408; e-mail rmho@mx.nthu.edu.tw.

10.1021/ma0526342 CCC: $33.50
Published on Web 03/17/2006

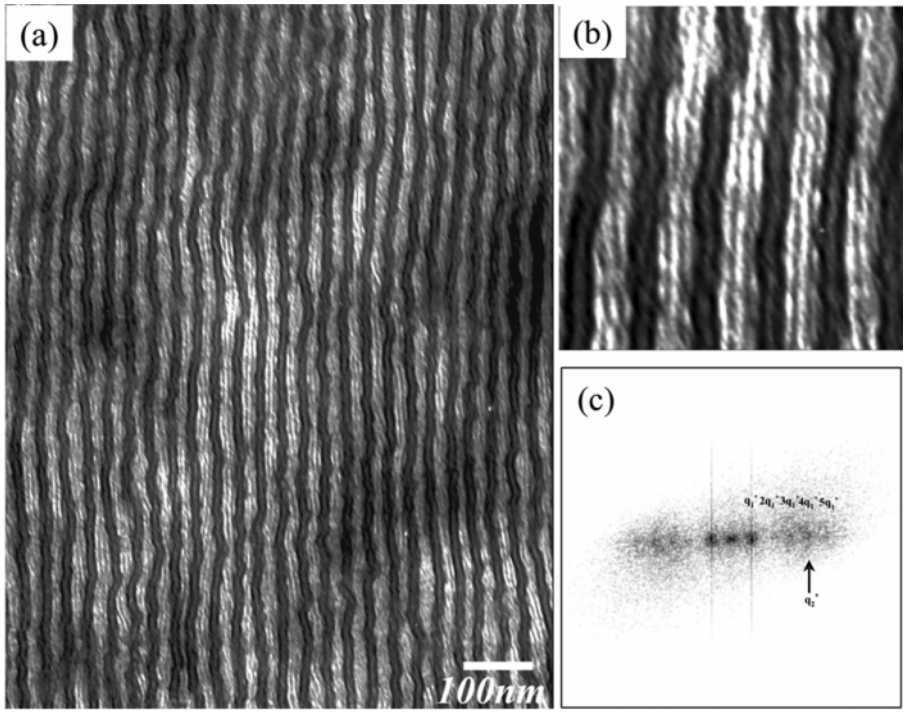

Figure 1. (a) TEM image of a thin section of oriented PS-sPP after sPP crystallized at 50 °C for 10 min from microphase-separated ordered melt at 180 °C, stained with RuO_4 for 30 min. (b) A magnification of one part of TEM image in which discrete trilayer sPP crystalline lamellae under confinement is observed. (c) Fast Fourier transform patterns of the TEM image.

dense sPP crystallites. The black borders between PS and sPP microdomains are not attributed to the defocusing effect as evidenced by through-focusing experiments (not shown), demonstrating that the black borders always remain at different focusing conditions. We speculate that the significant contrast is attributed to the enhanced staining effect on the interphase between PS and sPP microdomains for microsectioned samples due to modulus discrepancy under cutting where residual stress may retain after microsection. Also, tilting experiments have been conducted (not shown), and similar results were obtained. The lamellar normal of the double-length-scale multilayered morphology was found to be perpendicular to the shear plane. It is noted that the observed morphology is different than the results in our previous report at which no significant trilayer crystalline lamellae can be clearly identified.[16] We speculate that the discrepancies in the TEM micrographs for the stained textures are attributed to the well-defined microstructure in oriented samples as compared to the randomly distributed lamellar microdomains in a previous study. Consequently, a much stronger mass−thickness contrast for TEM imaging in this study was achieved due to the enhancement of staining effect in the crystallized, oriented sPP microdomains so as to truly resolve the microdomains for amorphous PS, crystallized, and amorphous sPP regions. Further experiments are necessary to clarify the improvement in staining effect due to the consequence of induced orientation. Similar results can be also observed for PS−sPP samples crystallized at temperatures of 65 and 80 °C even at 100 °C where crystallization leads to breakout morphology.

Figure 2 shows the time evolution of 1D SAXS profiles for PS−sPP quenched from microphase-separated ordered melt (ca. 180 °C) to 50 °C. No appreciable displacement in the low q scattering peaks (attributed to the microphase-separated microdomains) during crystallization was found, implying confined crystallization. After the completion of crystallization, an extra peak appeared at higher q value. The intensity of this peak gradually increased as the progress of crystallization, and the

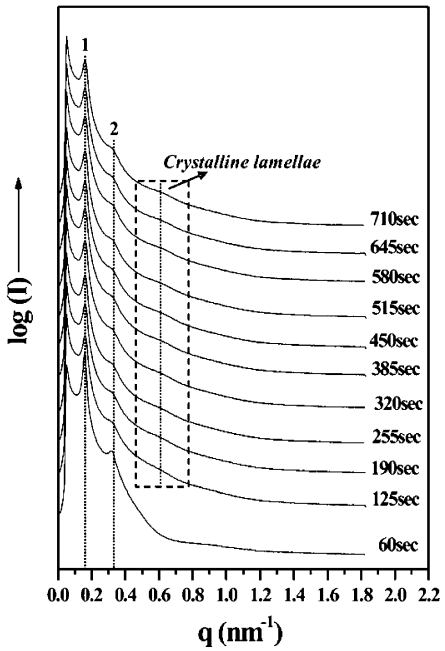

Figure 2. Time-resolved 1D SAXS profiles of PS−sPP isothermally crystallized at 50 °C for different isothermal times from microphase-separated ordered melt at 180 °C.

scattering peaks were diminished once the sample temperature was raised above the melting of sPP, suggesting that the peak is attributed to the growth of sPP crystalline lamellae in a confined environment instead of the fourth order of scattering peak due to microphase-separated microstructure. Also, the results of fast Fourier transform (FFT) of the TEM image (Figure 1c) were similar to that of 1D SAXS profiles (Figure 2). As observed, the double-length-scale multilayered morphology in the TEM micrograph resulted in two sets of FFT scattering patterns: a set of low q ratio diffractions with 1:2:3:4:5 attributed to the ordered microphase-separated lamellae and a high q value

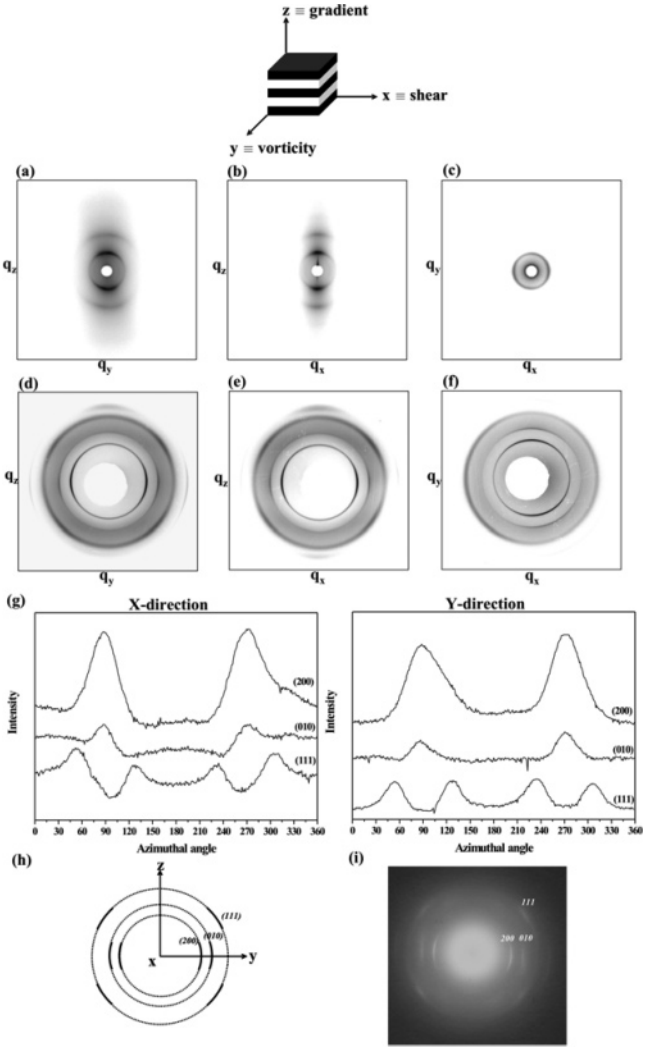

Figure 3. X-ray scattering patterns of oriented PS−sPP samples isothermally crystallized at 50 °C from microphase-separated ordered melt at 180 °C: (a) 2D SAXS obtained when X-ray beam is along *x*-direction; (b) 2D SAXS along *y*-direction; (c) 2D SAXS along *z*-direction; (d) 2D WAXD along *x*-direction; (e) 2D WAXD along *y*-direction; (f) 2D WAXD along *z*-direction; (g) azimuthal scanning profiles of the (200), (010), and (111) reflections of the 2D WAXD pattern; (h) schematic of the 2-D WAXD pattern; (i) SAED pattern obtained from the microsections of the crystallized samples (that is, the oriented samples of Figure 1 but without staining).

attributed to the periodic sPP crystalline lamellae. Consistently, the scattering periodicities appearing in SAXS results (Figure 2) are exactly the same with the scattering analysis from the morphological observations, further confirming the formation of trilayer sPP crystalline lamellae under confinement in between the vitrified PS microdomains.

To study the crystallographic details of crystalline sPP crystallites under confinement, the oriented samples of microphase-separated microdomains were prepared as described above. The shear-aligned and then crystallized samples were examined by the combined two-dimensional (2D) SAXS and WAXD measurements. Figure 3a−c shows 2D SAXS patterns taken along the shear, the vorticity, and the gradient directions designated as *x*, *y*, and *z*, respectively. The strong anisotropy in these patterns indicates that oriented microphase-separated lamellar microdomains were obtained after the shearing process. For SAXS patterns along the *x* and *y* directions, both patterns are practically identical, showing typical scattering results for distinct microphase-separated lamellar morphology with a q^* ratio of 1:2 being observed. By contrast, only a weak isotropic SAXS diffraction in the 2D SAXS pattern along the *z* direction (i.e., parallel to the gradient direction) was observed. Consistent with TEM observations, the microphase-separated lamellar normal of shear aligned samples appeared as preferred orientation along the *z*-axis. The corresponding 2D WAXD results along the *x*, *y*, and *z* directions (Figure 3d−f) on the aligned sample were also obtained. Similar to the SAXS results, these results indicate that the sPP crystallites under hard confinement form specific crystalline orientation with respect to the shear-induced oriented microphase-separated lamellar microdomains. On the basis of the orthorhombic lattice structure of sPP crystals, a helical disordered form I structure with typical unit cell dimensions of $a = 1.45$ nm, $b = 0.56$ nm, $c = 0.74$ nm and $\alpha = \beta = \gamma = 90°$,[20] the observed reflections could be indexed as (200), (010), and (111). The azimuthal profiles of these reflections (Figure 3g) were obtained from the 2D WAXD pattern (Figure 3d,e). It is seen that the maximum diffraction intensity of the (200) and (010) reflection locates at azimuthal angle $\Phi = 90°$ and 270° and of the (111) reflection at $\Phi = 55°$, 125°, 235°, and 305°. The schematic 2D WAXD pattern is illustrated in Figure 3h, which is consistent with a typical fiber diffraction pattern along *z*-axis. Combining the corresponding SAXS and WAXD scattering results, the specific scattering features suggest an in-plane orientation for the crystalline sPP at which the molecular chains of crystalline sPP are perpendicular to the microphase-separated lamellae, as illustrated in Figure 4. To further confirm the specific crystallographic geometry of the crystalline sPP under confinement, electron diffraction experiments were carried out on the microsections of the crystallized samples (that is, the oriented samples of Figure 1 but without staining). Figure 3i shows the selected area electron diffraction results of the crystallized samples, and the results are in line with that of the X-ray scattering measurements (Figure 3h). Although the dark field TEM imaging of the sPP crystallites was not able to be acquired due to the sensitive crystalline sPP with respect to electron beam damage, we can still recognize that the electron diffractions are resulted from the oriented sPP crystallites of which flashing stripes can be frequently observed by direct observations. These observations thus concluded that the trilayer crystalline sPP lamellae are intrinsically formed, and the molecular chains of

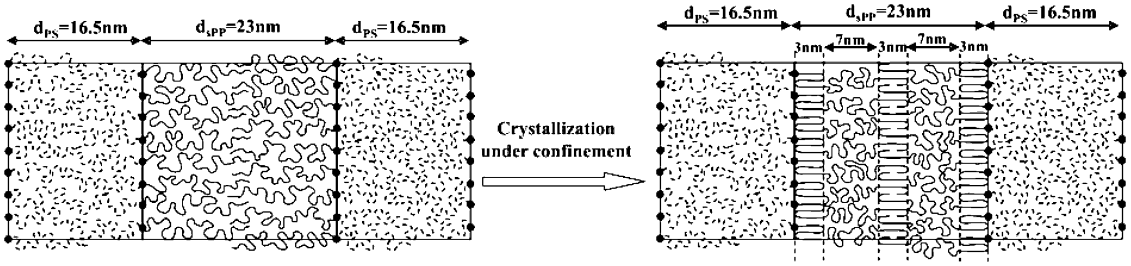

Figure 4. Schematic representation of the chain dispositions of trilayer sPP crystalline lamellae under the confinement of vitrified PS.

the sPP crystallites appear as perpendicular type to the microphase-separated lamellae.

As observed, the microphase-separated lamellar microdomains and the formed sPP crystalline lamellae were both oriented. The oriented microphase-separated lamellae are attributed to the shear-induced orientation. By contrast, the specific crystallographic geometry of the sPP crystalline lamellae is intuitionally originated by the spatially confined environment. From 1D SAXS profiles in Figure 2, the long period of microphase-separated lamellae was determined as ca. 39.5 nm. On the basis of the determined long period and the volume fraction of sPP block (f_{sPP}^{v}), the self-assembled lamellar thickness of the sPP block (d_{sPP}) was determined as 23.0 nm. Also, the long period of sPP crystalline lamellae was determined as ca. 10.0 nm. The volume fraction crystallinity of sPP crystallites was estimated as ca. 38.7% by differential scanning calorimetry measurements, which is approximately consistent to the crystallinity measured by wide-angle X-ray diffraction. Combining the results of crystallographic studies (a perpendicular type of molecular chain dispositions in crystalline sPP) and the measured crystallinity, the crystalline lamellar thickness of sPP crystallites was determined as ca. 3.0 nm according to the densities of crystalline sPP ($\rho_c = 0.9$ g/cm^3) and amorphous sPP ($\rho_a = 0.854$ g/cm^3) on the assumptions of one-dimensional density profile for the sPP crystallites (see Figure 4 for the schematic picture). In fact, the determined thickness of sPP crystalline lamellae is roughly in line with the melting temperature estimated from sPP homopolymers.[21] As a result, the molecular dispositions of the sPP crystalline lamellae under confinement are illustrated in Figure 4. As shown, the trilayer sPP crystalline lamellae are formed within the confined microdomains and grown as equivalent crystalline thickness. On the basis of simple geometric argument (we know the number of repeat units and the crystalline thickness as well as the crystalline lamellar spacing) and the crystallinity value, the sPP molecular chains in the crystalline phase roughly appear as three-chain-traverse crystalline lamellae near the edge of sPP microdomain and one and a half chain-traverse crystalline lamellae in the middle of sPP microdomain for one single sPP chain. In addition, we calculate the reduced tethering density (ca. 24.4) according to the proposed schematic illustration on the basis of tethering definition.[22] Those results suggest that the sPP chains in the microphase-separated microdomains indeed appear as highly stretched chains under thermodynamic consideration. This may explain the occurrence of specific crystalline orientation (that is, perpendicular orientation) with respect to the PS layer where the orientation might be initiated from the highly stretched sPP chains. To our knowledge, this unique morphology has not been observed in polymeric crystallization under confinement. The origins for the formation of the trilayer crystalline lamellar morphology remain an open question, and a detailed mechanism for the growth of the specific morphology is still under examination.

Acknowledgment. R.M.H. and J.C.T. acknowledge the financial support of the National Science Council (NSC) of Taiwan (NSC-93-2216-E-110-001, NSC-92-2216-E-110-009, and NSC-91-2216-E-194-003). B.H. acknowledges the partial financial support of this work provided by the National Science Foundation (DMR-0405432) and Dr. Y.-S. Sun of the National Synchrotron Radiation Research Center for their help in Synchrotron SAXS experiments. R.M.H. also thanks Ms. P.-C. Chao of the Regional Instruments Center at NCHU for her help in TEM experiments.

References and Notes

(1) Whitesides, G. M.; Grzybowski, B. *Science* **2002**, *295*, 2418.
(2) De Rosa, C.; Park, C.; Thomas, E. L.; Lotz, B. *Nature (London)* **2000**, *405*, 433. (b) Reiter, G.; Gastelein, G.; Hoerner, P.; Riess, G.; Blumen, A.; Sommer, J.-U. *Phys. Rev. Lett.* **1999**, *83*, 3844. (c) Ho, R.-M.; Hsieh, P.-Y.; Tseng, W.-H.; Lin, C. C.; Huang, B. H. *Macromolecules* **2003**, *36*, 9085.
(3) Ryan, A. J.; Hamley, I. W.; Bras, W.; Bates, F. S. *Macromolecules* **1995**, *28*, 3860. (b) Yang, Y.-W.; Tanodekaew, S.; Mai, S.-M.; Booth, C.; Ryan, A. J.; Bras, W.; Viras, K. *Macromolecules* **1995**, *28*, 6029. (c) Zhu, L.; Chen, Y.; Zhang, A.; Calhoun, B. H.; Chun, M.; Quirk, R. P.; Cheng, S. Z. D.; Hsiao, B. S.; Yeh, F.; Hashimoto, T. *Phys. Rev. B* **1999**, *60*, 10022.
(4) Loo, Y.-L.; Register, R. A.; Ryan, A. J. *Macromolecules* **2002**, *35*, 2365. (b) Xu, J.-T.; Fairclough, J. P. A.; Mai, S.-M.; Ryan, A. J.; Chaibundit, C. *Macromolecules* **2002**, *35*, 6937.
(5) Douzinas, K. C.; Cohen, R. E. *Macromolecules* **1992**, *25*, 5030.
(6) Hamley, I. W.; Fairclough, J. P. A.; Terrill, N. J.; Ryan, A. J.; Lipic, P. M.; Bates, F. S.; Towns-Andrews, E. *Macromolecules* **1996**, *29*, 8835.
(7) Quiram, D. J.; Register, R. A.; Marchand, G. R.; Adamson, D. H. *Macromolecules* **1998**, *31*, 4891.
(8) (a) Zhu, L.; Cheng, S. Z. D.; Calhoun, B. H.; Ge, G.; Quirk, R. P.; Thomas, E. L.; Hsiao, B. S.; Yeh, F.; Lotz, B. *J. Am. Chem. Soc.* **2000**, *122*, 5957. (b) Zhu, L.; Cheng, S. Z. D.; Calhoun, B. H.; Ge, Q.; Quirk, R. P.; Thomas, E. L.; Hsiao, B. S,; Yeh, F.; Lotz, B. *Polymer* **2001**, *42*, 5829.
(9) Loo, Y.-L.; Register, R. A.; Ryan, A. J. *Phys. Rev. Lett.* **2000**, *84*, 4120.
(10) Kofinas, P.; Cohen, R. E. *Macromolecules* **1994**, *27*, 3002.
(11) Quiram, D. J.; Register, R. A.; Marchand, G. R. *Macromolecules* **1997**, *30*, 4551.
(12) Chen, H. L.; Hsiao, S. C.; Lin, T. L.; Yamauchi, K.; Hasegawa, H.; Hashimoto, T. *Macromolecules* **2001**, *34*, 671.
(13) Loo, Y.-L.; Register, R. A.; Ryan, A. J.; Dee, G. T. *Macromolecules* **2001**, *34*, 8968.
(14) Xu, J.-T.; Turner, S. C.; Fairclough, J. P. A.; Mai, S.-M.; Ryan, A. J.; Chaibundit, C.; Booth, C. *Macromolecules* **2002**, *35*, 3614.
(15) Ho, R.-M.; Lin, F.-H.; Tsai, C.-C.; Lin, C.-C.; Ko, B.-T.; Hsiao, B. S.; Sics, I. *Macromolecules* **2004**, *37*, 5985.
(16) Ho, R.-M.; Chung, T.-M.; Tsai, J.-C.; Kuo, J.-C.; Hsiao, B. S.; Sics, I. *Macromol. Rapid Commun.* **2005**, *26*, 107.
(17) (a) Rangarajan, P.; Register, R. A.; Fetters, L. J. *Macromolecules* **1993**, *26*, 4640. (b) Ryan, A. J.; Fairclough, J. P. A.; Hamley, I. W.; Mai, S.-M.; Booth, C. *Macromolecules* **1997**, *30*, 1723. (c) Lee, L.-B. W.; Register, R. A. *Macromolecules* **2004**, *37*, 7278.
(18) Tsai, J.-C.; Kuo, J.-C.; Ho, R.-M.; Chung, T.-M. *Macromolecules*, in press.
(19) (a) Khan, S. A.; Larson, R. G. *Rheol. Acta* **1991**, *30*, 1. (b) Lee, H. H.; Register, R. A.; Hajduk, D. A.; Gruner, S. M. *Polym. Eng. Sci.* **1996**, *36*, 1414.
(20) (a) Lotz, B.; Lovinger, A. J.; Cais, R. E. *Macromolecules* **1988**, *21*, 2375. (b) Lovinger, A. J.; Lotz, B.; Davis, D. D.; Padden, F. J. *Macromolecules* **1993**, *26*, 3494. (c) De Rosa, C.; Corradini, P. *Macromolecules* **1993**, *26*, 5711.
(21) Schmidtke, J.; Strobl, G.; Thurn-Albrecht, T. *Macromolecules* **1997**, *30*, 5804.
(22) (a) Chen, W. Y.; Zheng, J. X.; Cheng, S. Z. D.; Li, C. Y.; Huang, P.; Zhu, L.; Xiong, H.; Ge, Q.; Guo, Y.; Quirk, R. P.; Lotz, B.; Deng, L.; Wu, C.; Thomas, E. L. *Phys. Rev. Lett.* **2004**, *93*, 28301. (b) Zheng, J. X.; Xiong, H.; Chen, W. Y.; Lee, K.; Van Horn, R. M.; Quirk, R. P.; Lotz, B.; Thomas, E. L.; Shi, A.-C.; Cheng, S. Z. D. *Macromolecules* **2006**, *39*, 641.

MA0526342